Available online at www.sciencedirect.com
ScienceDirect
Acta Materialia 58 (2010) 2708–2715
Acta MATERIALIA
www.elsevier.com/locate/actamat

Experimental and computational study on the effect of yttrium on the phase stability of sputtered Cr–Al–Y–N hard coatings

F. Rovere [a,b,*], D. Music [b], J.M. Schneider [b], P.H. Mayrhofer [a]

[a] Department of Physical Metallurgy and Materials Testing, Montanuniversität Leoben, A-8700 Leoben, Austria
[b] Materials Chemistry, RWTH Aachen University, D-52056 Aachen, Germany

Received 30 November 2009; received in revised form 30 December 2009; accepted 5 January 2010
Available online 1 February 2010

Abstract

The effect of Y incorporation into cubic Cr–Al–N (B1) was studied using ab initio calculations, X-ray diffraction and energy-dispersive X-ray analysis of sputtered quaternary nitride films. The data obtained indicate that the Y incorporation shifts the critical Al content, where the hexagonal (B4) structure is stable, to lower values. The calculated critical Al contents of $x \approx 0.75$ for $Cr_{1-x}Al_xN$ and $x \approx 0.625$ for $Cr_{1-x-y}Al_xY_yN$ with $y = 0.125$ are consistent with experimentally obtained values of $x = 0.69$ for $Cr_{1-x}Al_xN$ and $x = 0.68$ and 0.61 for $Cr_{1-x-y}Al_xY_yN$ with $y = 0.02$ and 0.06, respectively. This may be understood based on the electronic structure. Both Cr and Al can randomly be substituted by Y. The substitution of Cr by Y increases the phase stability due to depletion of non-bonding (anti-bonding) states, while the substitution of Al by Y decreases the phase stability mainly due to lattice strain.

Keywords: CrAlN; Phase stability; Ab initio; OpenMX

1. Introduction

Among the various transition metal nitride-based hard coatings which have been employed for materials protection, metastable cubic $Cr_{1-x}Al_xN$ films have become increasingly important due to their excellent physical, chemical and mechanical properties, such as high hardness, good wear resistance, and promising corrosion and oxidation resistance [1–10]. $Cr_{1-x}Al_xN$ can be synthesized by physical vapor deposition (PVD) in its metastable face-centered cubic (fcc) B1 structure (space group Fm-3m, NaCl prototype) up to a critical Al content, where the hexagonal closed-packed (hcp) B4 structure (space group $P6_3mc$, wurtzite prototype) becomes energetically favorable. Since the nucleation of the hcp B4 structure is connected with undesirable coating performances, the fcc B1 structure is usually preferred for wear protection applications [7,11].

Experimentally obtained critical Al contents where B1/B4 transition occurs are reported from $x = 0.60$ to 0.75 [7,12–18]. Based on the calculation of band parameters [19] and on thermodynamic calculations [20], critical Al contents of $x = 0.772$ and 0.815 were reported, respectively. This considerable spread may be related to the significant impact of deposition conditions on the defect structure of a material system with an endothermic mixing enthalpy [18]. Based on ab initio calculations of a large number of different ad hoc supercells with varying metal sublattice populations, it was shown that a variation in the configurational contribution to the total energy results in a spread of predicted critical Al content of $x = 0.48$–0.75 [18].

Yttrium-containing cubic (B1) $Cr_{1-x}Al_xN$ films, i.e. $(Cr_{1-x}Al_x)_{1-y}Y_yN$, were shown to exhibit improved oxidation resistance compared to Y-free ternary films when the Y content did not exceed ~1 at.% (2 mol.% YN) [21]. In such coatings, Y promotes the formation of a dense and adherent mixed $Al_2O_3 + Cr_2O_3$ scale which results in a very

* Corresponding author. Address: Department of Physical Metallurgy and Materials Testing, Montanuniversität Leoben, A-8700 Leoben, Austria.
E-mail address: florian.rovere@mu-leoben.at (F. Rovere).

1359-6454/$36.00
doi:10.1016/j.actamat.2010.01.005

promising oxidation resistance up to temperatures exceeding 1000 °C. Higher Y contents improve the thermal stability and thermomechanical properties (higher hardness at lower stress levels), suggesting a retarding effect of Y on diffusion-driven processes (retarded decomposition fcc CrAlN → hcp Cr_2N + hcp AlN + N_2 → bfcc Cr + hcp AlN + N_2) [22], but are also detrimental to the oxidation resistance as the transformation of fast-growing, non-protective alumina polymorphs (γ, θ) to stable, protective α-Al_2O_3 is impeded [21,23]. However, fcc (B1) $Cr_{1-x}Al_xN$-based coatings with Y contents of ~1 at.% show very promising results in dry milling applications or as protective coating for substrates susceptible to high-temperature oxidation, such as γ-TiAl-based alloys [24–26]. Assuming that Y may substitute Cr and Al equally, the notation $Cr_{1-x-y}Al_xY_yN$ instead of $(Cr_{1-x}Al_x)_{1-y}Y_yN$ is used below for convenience, as the individual contents of Cr, Al and Y can thereby be directly assessed.

For $Ti_{1-x}Al_xN$ films isostructural to $Cr_{1-x}Al_xN$, the incorporation of 6.25 at.% Y (12.5 mol.% YN) results in a decrease in the predicted critical Al content where B1/B4 transition occurs from $x = 0.69$ to 0.56, as obtained by ab initio calculations [27]. Moreover, experimental investigations indicate that for an addition of only 1.5 at.% of Y (3 mol.% YN) a mixed B1/B4 structure is formed for an Al content of $x = 0.56$. Hence, any beneficial effects of Y addition on the oxidation resistance of such coatings are at the expense of the mechanical properties as the crystallization of the B4 structure is usually connected to lower hardness and wear resistance [7,28]. Consequently, improvements in the mechanical and chemical properties of $Cr_{1-x-y}Al_xY_yN$-based coatings may be obtained by selecting a suitable Y content, which was found to be ⩽1 at.% (2 mol.% YN) [21], while at the same time maximizing the Al content before nucleation of the B4 structure occurs.

Here, we use ab initio calculations together with experimental investigations of sputtered $Cr_{1-x-y}Al_xY_yN$ films to investigate the effect of Y incorporation on the critical Al content x, where the B4 structure becomes energetically favorable over the B1 structure. This may be understood by considering the electronic structure. Assuming that both Cr and Al can be randomly substituted by Y, the substitution of Cr by Y increases the phase stability due to depletion of non-bonding (anti-bonding) states, while the substitution of Al by Y decreases the phase stability mainly due to lattice strain. Moreover, the substitution of Al by Y in B1 is energetically less favorable than in B4 due to lattice strain. Hence, Y decreases the critical Al contents in these cubic ternary nitrides. Furthermore, the impact of Y on the mechanical properties and the retarding effect of Y incorporation on diffusion-driven processes are discussed.

1.1. Computational details

The ab initio calculations in this work were carried out using the open source package for material explorer (openMX), a program package which is based on density functional theory (DFT) [29] and basis functions in the form of linear combinations of localized pseudoatomic orbitals [30]. The electronic potentials are fully relativistic with partial core corrections [31,32] and the generalized gradient approximation (GGA) is applied [33]. The basis functions are generated by a confinement scheme [30,34] and specified as follows: Cr8.0-*s*2*p*2*d*1, Al6.0-*s*3*p*2*d*1, N5.5-*s*2*p*1 and Y6.5-*s*3*p*2*d*1. The first symbol designates the chemical name, followed by the cutoff radius (in Bohr radius) in the confinement scheme and the last set of symbols defines the primitive orbitals applied. The energy cutoff (160 ± 5 Ryd) and the *k*-point grid (3 × 3 × 3) within the real space grid technique [35] were adjusted to reach a numerical precision of 10^{-5} H atom^{-1}. For the fcc B1 (NaCl prototype) structure, two types of supercells (four unit cells in a 2 × 2 × 1 array) containing 32 atoms were calculated: an ad hoc configuration, where the positions of Cr and Al ions at the metal sublattice were randomly chosen, and a configuration following the special quasirandom structures (*SQS*) concept of Zunger et al. [36]. The *SQS* implementation via the short-range order parameter (SRO) is available within the local self-consistent Green's function software package [37,38]. The Warren–Cowley SRO parameter [39] within three coordination shells was used to account for randomness in the metal sublattice. For the hcp B4 (wurtzite) structure (eight unit cells in a 2 × 2 × 2 array, 32 atoms) ad hoc and *SQS* configurations were also considered. All cells were relaxed with respect to atomic positions and cell volumes. To describe the magnetic effects on the total energy [40] a fully non-collinear DFT, including spin–orbit coupling as implemented in the openMX code, was used [41–45]. The initial occupations for the up and down spins of the 14 valence electrons considered for Cr (3*s*, 3*p*, 3*d* and 4*s* orbitals) were nine and five, respectively. Furthermore, the *SQS* implementation mentioned above was used to simulate antiferromagnetic spin polarization with a random up and down spin arrangement. The energies of formation were calculated with respect to the elements. Therefore, the total energies of Al, Cr and Y were calculated for their unit cells, while the total energy of N was calculated for an N_2 molecule. The lattice parameters, total energies and bulk moduli were obtained by least-squares fits of the calculated total energies over lattice parameter curves employing the Birch–Murnaghan equation of state [46].

2. Experimental details

$Cr_{1-x-y}Al_xY_yN$ films were grown on polished Si(1 0 0)-substrates (20 × 7 × 0.35 mm) in a laboratory-scale unbalanced direct current magnetron sputtering system. The film deposition was carried out in an Ar + N_2 atmosphere (both of 99.999% purity). Powder metallurgically produced targets (Ø75 × 6 mm, PLANSEE) with Y contents of 0, 2, 4 and 8 at.% and an Al/Cr ratio of 1.5 were used. The Al content x was varied by placing additional Al (99.999%

purity) disks (Ø5 × 2 mm) in the sputtering erosion tracks of the targets. The base pressure in the system was below 1 mPa and the total working gas pressure during deposition was kept constant at 0.4 Pa with an N_2 partial pressure of ~35%. The magnetron's power density was ~6.8 W cm^{-2} and the substrate temperature was set to ~475 °C. The target–substrate distance was 50 mm. All depositions were carried out at a floating potential of −25 V.

Structural investigations of the films were conducted by X-ray diffraction (XRD), using a Bruker D8 diffractometer with a SolX detector in the Bragg–Brentano configuration with Cu Kα radiation ($\lambda = 1.54056$ nm). For the identification of the B4 structure, the pattern 25-1133 for hcp AlN of the JCPDS database was used. The chemical compositions were determined using energy-dispersive X-ray analysis (EDX; Oxford Instruments Inc.) in a Zeiss Evo 50 scanning electron microscope. For EDX calibration a Co standard was used. Quantification was conducted using standards for Cr, Al (Al_2O_3), Y and N (TiN).

3. Results and discussion

We start the discussion by analyzing the binary counterparts. Table 1 summarizes ab initio calculated lattice parameter and bulk modulus data for the metals and binary metal nitrides considered here as compared to experimental and calculated values reported elsewhere. For the metals, excellent agreement is obtained for equilibrium lattice parameters (difference less than 1%) as well as for bulk moduli (difference less than 15%). For the binary metal nitrides, the calculated equilibrium lattice parameters are slightly overestimated (difference less than 3%), but the calculated bulk moduli are nevertheless well within the range of previously reported values. Moreover, the GGA exchange–correlation functional is known to yield slightly overestimated lattice constants. Consequently, the employed pseudopotentials generally yield good consistency between the data calculated in this work and the data from the literature.

Table 1
Ab initio calculated lattice parameter a_c and bulk modulus B_c data for the metals (M) and metal nitrides (MN) considered as compared to experimental and calculated values reported elsewhere (a_r and B_r).

M/MN	Lattice parameter (Å)	Bulk modulus (GPa)
Al (fcc)	$a_c = 4.05$ $a_r = 4.049$ [76]	$B_c = 79.4$ $B_r = 75.2$ [77]
Cr (bcc)	$a_c = 2.92$ $a_r = 2.895$ [76]	$B_c = 156.8$ $B_r = 160$ [77]
Y (hcp)	$a_c = 3.63$ ($c/a = 1.55$) $a_r = 3.647$ ($c/a = 1.57$) [76]	$B_c = 47.4$ $B_r = 41.2$ [77]
AlN (fcc)	$a_c = 4.13$ $a_r = 4.045$, 4.12 [76], 4.094 [40]	$B_c = 262.2$ $B_r = 174$–329 [78], 252 [18]
AlN (hcp)	$a_c = 3.18$ ($c/a = 1.61$) $a_r = 3.11$ ($c/a = 1.60$) [76], 3.157 [79]	$B_c = 198.1$ $B_r = 185$–208 [18,61,80]
CrN (fcc) (AFM)	$a_c = 4.22$ $a_r = 4.148$ [76], 4.162 [81], 4.185 [82], 4.206 [40]	$B_c = 277.7$ $B_r = 245$ [18]
CrN (hcp)	$a_c = 3.19$ ($c/a = 1.62$) $a_r = 3.111$ ($c/a = 1.64$) [18]	$B_c = 185.6$ $B_r = 188$ [18]
YN (fcc)	$a_c = 4.99$ $a_r = 4.76$–4.93 [83], 4.89 [76]	$B_c = 151.4$ $B_r = 145$–187 [83]
YN (hcp)	$a_c = 3.83$ ($c/a = 1.57$) $a_r = 3.67 - 3.78$ ($c/a = 1.58$–1.62) [83]	$B_c = 112.6$ $B_r = 110$–139 [83]

For cubic (fcc) CrN, the antiferromagnetic (AFM) configuration with a random spin up and down arrangement (see computational details) yields an energy of formation E_f of −1.511 eV atom^{-1}, which is smaller than a ferromagnetic (FM) spin arrangement by 0.053 eV atom^{-1} and smaller than a nonmagnetic (NM) configuration by 0.272 eV atom^{-1}. While the total E_f values are somewhat larger than the values reported in Ref. [18], the differences between the AFM, FM and NM configurations are in good agreement with the values in Refs. [18,40]. Moreover, the lattice parameter variation of 4.22, 4.25 and 4.14 Å obtained here for cubic CrN in the AFM, FM and NM configurations, respectively, is consistent with the ~4.20, 4.22 and 4.13 Å for the AFM, FM and NM configurations, respectively, obtained in Ref. [40].

For polycrystalline CrN, a magnetic stress-induced structural modification from cubic to orthorhombic is observed during the transition of the high-temperature paramagnetic (PM) state to the low-temperature AFM state when the temperature is below the Néel temperature [47,48]. However, the difference in E_f between the orthorhombic and the cubic AFM configurations was shown to be negligible [18]. Furthermore, Alling et al. [40] reported that there is no significant difference in lattice parameter and E_f between the AFM and PM configurations of cubic $Cr_{1-x}Al_xN$ when disordered magnetic moments are used to describe the PM state. Consequently, the AFM configuration with random spin up and down states is considered here for further discussion. Nevertheless, it should be noted that not considering the magnetic moment (NM configuration) will lead to larger deviations from experiments. The effective magnetic moment per Cr atom calculated for the AFM configuration is 2.82 μ_B, which is in the range of reported values of 2.17–3.17 μ_B [40,47,49–53].

Before discussing the final quaternary configuration, we consider all ternary phases, i.e. CrN–YN, AlN–YN and CrN–AlN solutions, to identify the electronic contributions needed for analyzing the quaternary data. Fig. 1 shows ab initio calculated E_f data for CrYN (open symbols) and AlYN (solid symbols). For the CrN and YN binaries, the fcc (B1) structure is obtained as the equilibrium ground state configuration. Consequently, the B1 structure is denoted as the equilibrium ground state configuration also for ternary CrYN. For that reason, the calculation of hcp (B4) CrYN is omitted here. The positive deviation from the

mechanical mixture (the line connecting fcc CrN and fcc YN), which indicates repulsive forces between the binary compounds and hence a system characterized by an endothermic mixing enthalpy, is mainly attributed to size effects. An electronic structure contribution due to the localization of *d*-states, which causes a high density of states at the Fermi level E_F [54,55] and was shown to be a destabilizing factor [55,56], may be excluded as both Cr ([Ar]$3d^5 4s$) and Y ([Kr]$4d5s^2$) exhibit *d* electrons. As discussed below, the Y incorporation into CrN rather increases the overall phase stability due to electronic effects. The strain caused by different lattice parameters of the binary constituents (see Table 1) can be qualitatively described by [57]:

$$\varepsilon = (1-y)\cdot|\delta_A| + y\cdot|\delta_B| \quad (1)$$

$$\text{with } \delta_A = \frac{V_V - V_{CrN}}{V_V} \quad \text{and} \quad \delta_B = \frac{V_V - V_{YN}}{V_V} \quad (2)$$

where V_V, V_{CrN} and Y_{YN} designate the equilibrium volumes for fcc $Cr_{1-y}Y_yN$ (as calculated by Vegard's law), fcc CrN and fcc YN, respectively. At a Y concentration of $y = 0.5$, where maximum lattice distortion occurs, a lattice strain $\varepsilon_{0.5}$ of 25% is obtained. Nevertheless, the substitution of Cr by Y in fcc CrYN continuously decreases the energy of formation until it reaches −3.01 eV atom^{-1} of fcc YN. The decreasing energy of formation suggests that Y incorporation increases the overall compound stability (cohesive energy), which is consistent with decomposition temperatures of 2674 and 1050 °C for YN and CrN [58], respectively. The higher stability of YN compared to CrN is attributed to the filling of the six bonding states of the hybridized non-metal *p*, metal *s* and metal *d* states (sp^3d^2 hybridization) by one 4*d* electron and two 5*s* electrons of Y together with three 2*p* electrons of N [59,60]. For CrN on the other hand, three surplus 3*d* electrons have to populate higher energetic non-bonding (anti-bonding) states, which is at the expense of the overall compound stability. Hence, when Y substitutes for Cr in CrYN, the stabilizing effect due to depletion of non-bonding states overcompensates the destabilizing effect of the accompanying lattice strain.

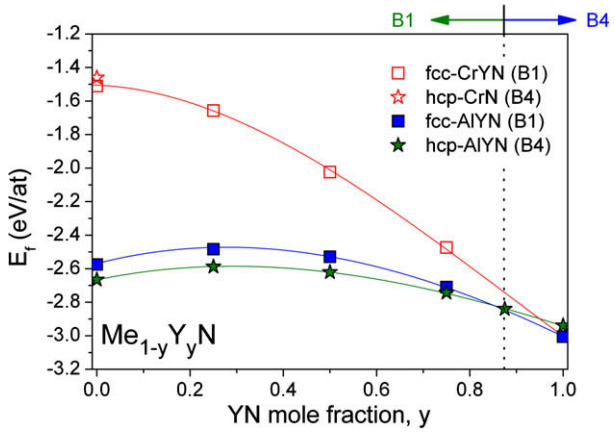

Fig. 1. Ab initio calculated energy of formation E_f data as a function of the YN mole fraction *y* for fcc (B1) $Cr_{1-y}Y_yN$, fcc (B1) $Al_{1-y}Y_yN$, hcp (B4) $Al_{1-y}Y_yN$ and hcp (B4) CrN, as obtained using *SQS* supercells.

In the case of AlYN, the hcp (B4) structure is obtained as the stable structural modification up to an YN mole fraction of $y \approx 0.875$, where the fcc (B1) modification of binary YN becomes more stable (see Fig. 1). For both the B1 (−2.58 eV atom^{-1}) and the B4 (−2.67 eV atom^{-1}) structural modifications, E_f initially increases with Y incorporation and with $y \geqslant 0.25$ it decreases down to −3.01 and −2.94 eV atom^{-1}, respectively. As AlN and YN are semiconductors [61,62] and therefore exhibit no populated states at E_F, a major contribution of the electronic configuration to the deviation from the mechanical mixture for AlYN (the line connecting fcc/hcp AlN and fcc/hcp YN) can also be excluded. Consequently, the initial increase in E_f for AlYN (see Fig. 1) may also be attributed mainly to lattice strain. For Y contents of $y = 0.5$, strain values of $\varepsilon_{0.5} = 28$ and 26% are obtained for the B1 and the B4 structure, respectively, suggesting that Y incorporation into the B4 structure is energetically slightly more favorable. This is consistent with mixing enthalpies ΔH_m, which are calculated after:

$$\Delta H_m(y) = E_{f,Me_{1-y}Y_yN} - [(1-y)E_{f,MeN} + yE_{f,YN}] \quad (3)$$

where $E_{f,Me1-yYyN}$, $E_{f,Me}$ and $E_{f,YN}$ designate the energies of formation of $Me_{1-y}Y_yN$ (Me = Cr, Al), MeN and YN, respectively (see Fig. 2). For the B1 and the B4 structural modifications of AlYN, maximum mixing enthalpies of 0.26 and 0.18 eV atom^{-1} are obtained, respectively. The similar mixing enthalpies obtained for the B1 structures of AlYN (0.26 eV atom^{-1}) and CrYN (0.24 eV atom^{-1}) furthermore indicate that Y would equally substitute Cr and Al in a cubic, quaternary CrAlYN compound, as expected. Nevertheless, as mentioned in the introduction, we chose the nomenclature $Cr_{1-x-y}Al_xY_yN$ for reasons of simplicity, as thereby the individual contents of the coating can be assessed directly. The overall large endothermic mixing enthalpies of AlYN and CrYN imply that the synthesis of single-phase films by conventional sputtering techniques may not be possible for high Y contents. This is consistent with reported amorphous microstructures of sputtered CrAlYN films with Y contents of 5.9 and 8.5 at.% (10.8 and 17.0 mol.% YN), which may be explained by the simultaneous crystallization of two different phases (fcc (B1) YN together with fcc (B1) CrAlN or hcp (B4) AlCrN) [63]. Endrino et al. [64] reported an amorphous structure for arc-deposited CrAlYN films with Y contents as low as 3.9 at.% (7.8 mol.% YN) contents of approximate 35 at.% ($x \approx 0.7$). On the other hand, we have shown in an earlier report [65] that incorporation of 4 at.% Y (8 mol.% YN) in CrAlN films with Al contents of 25 at.% ($x = 0.5$) yields a single-phase B1 structure.

Fig. 3 shows ab initio calculated E_f data for the fcc (B1) and the hcp (B4) structural modifications of (a) ternary CrAlN and (b) quaternary CrAlYN using ad hoc (open symbols) and *SQS* (solid symbols) supercells. For all supercells a Y content of 6.25 at.% (12.5 mol.% YN) is employed, which

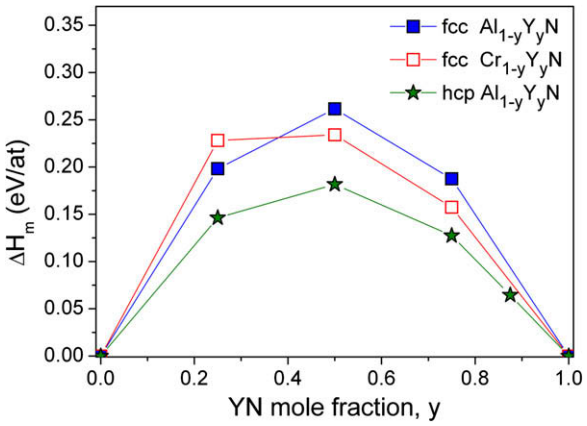

Fig. 2. Ab initio calculated mixing enthalpies ΔH_m of fcc (B1) $Al_{1-y}Y_yN$ (solid squares), hcp (B4) $Al_{1-y}Y_yN$ (solid stars) and fcc (B1) $Cr_{1-y}Y_yN$ (open squares), as obtained using *SQS* supercells.

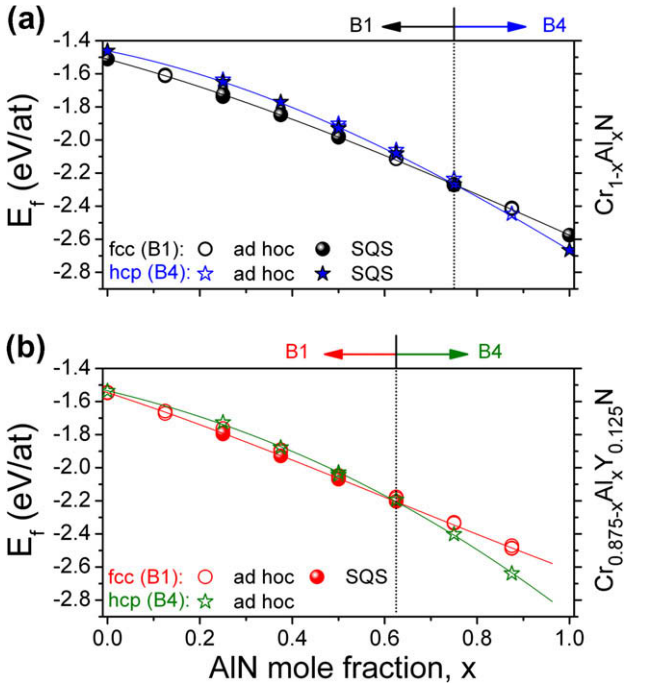

Fig. 3. Ab initio calculated energies of formation E_f as a function of the AlN mole fraction x for (a) fcc (B1) $Cr_{1-x}Al_xN$ (black circles) and hcp (B4) $Cr_{1-x}Al_xN$ (blue stars) and for (b) fcc (B1) $Cr_{0.875-x}Al_xY_{0.125}N$ (red circles) and hcp (B4) $Cr_{0.875-x}Al_xY_{0.125}N$ (green stars), as obtained using ad hoc and *SQS* supercells. (For interpretation of the references to colour in this figure legend, the reader is referred to the web version of this article.)

is considered as reasonably close to the maximum possible Y contents in experimentally achievable single-phase structures. The plotted third-order polynomials serve only as guidelines for the eye. Based on the data presented, the critical Al content where B1/B4 transition occurs is obtained at $x \approx 0.75$ (see Fig. 3a). This is consistent with reported computationally and experimentally obtained critical Al values of $x = 0.48$–0.815 [18–20] and $x = 0.60$–0.75 [7,12–17,55], respectively. However, if 6.25 at.% of Y (12.5 mol.% YN) is incorporated into CrAlN to form $Cr_{0.875-x}Al_xY_{0.125}N$, the critical Al concentration, where the B4 structure becomes more stable, decreases to $x \approx 0.625$. Furthermore, the Y incorporation of $y = 0.125$ decreases the energy of formation E_f of $Cr_{1-x-y}Al_xY_yN$ by 0.04 eV atom^{-1} at $x = 0.0$ up to maximum of 0.09 eV atom^{-1} at $x = 0.5$, which agrees well with the effect of Y in the ternary compounds CrYN and AlYN (see above). It is again noted that a decreasing energy of formation corresponds to an increasing compound stability (cohesive energy). The experimentally observed retarding effect of Y on diffusion-driven processes [22,26] may hence be explained in part by the increasing cohesive energy [59,60], which certainly increases the energies necessary to create defects or the migration energy itself [66]. On the other hand, it may be speculated that the diffusitivity is also affected by the incorporation of large particles. The ionic radii of Cr, Al and Y in 12-coordinated metals are 1.28, 1.43 and 1.80 Å, respectively [67].

To validate the theoretical data presented above, we compare these to experimental data obtained from the thin-films synthesized. Fig. 4a–c presents XRD data of experimentally synthesized CrAlYN films, where for different Y contents the Al content was systematically increased. Based on XRD and EDX analyses, critical Al contents of $x = 0.69$ for Y-free $Cr_{1-x}Al_xN$ and $x = 0.68$ and 0.61 for $y = 0.02$ and 0.06 Y-containing $Cr_{1-x-y}Al_xY_yN$ films are obtained, respectively. The comparison of experimentally determined and ab initio calculated critical compositions where B1/B4 transition occurs yields somewhat lower critical Al contents for the experiment (see Fig. 5). However, this can be explained by the effect of deposition conditions (such as ion flux and ion energy) on the metal sublattice population, affecting in turn the phase stability of experimentally grown films, as previously suggested for TiAlN [68] and CrAlN [18]. Moreover, defects in the non-metal sublattice (N-vacancies) have also been suggested to affect the phase stability [69]. Thus, crystallization of the B4 structure may occur below the theoretically predicted Al contents. The theoretical data presented are nevertheless consistent with the microstructure of a CrAlYN film with an Al content of $x \approx 0.7$ and a YN mole fraction of 7.8% reported in Ref. [64] (see Fig. 5). The simultaneous crystallization of B1 and B4 phases can certainly explain the nanocrystalline, partially X-ray-amorphous structure.

Fig. 6a and b summarizes the calculated lattice parameter and bulk modulus data of B1 CrAlN and CrAlYN with 6.25 at.% Y (12.5 mol.% YN) as a function of the AlN mole fraction. In agreement with experimental investigations, the incorporation of Al into CrN causes a decreasing lattice parameter whereas incorporation of Y into CrAlN increases it. As already discussed above, the employed pseudoatomic orbitals yield somewhat overestimated (max. 2%) lattice parameters for the metal nitrides considered here compared to the values reported in the literature, or the experimental values obtained here. However, the observed total change in lattice

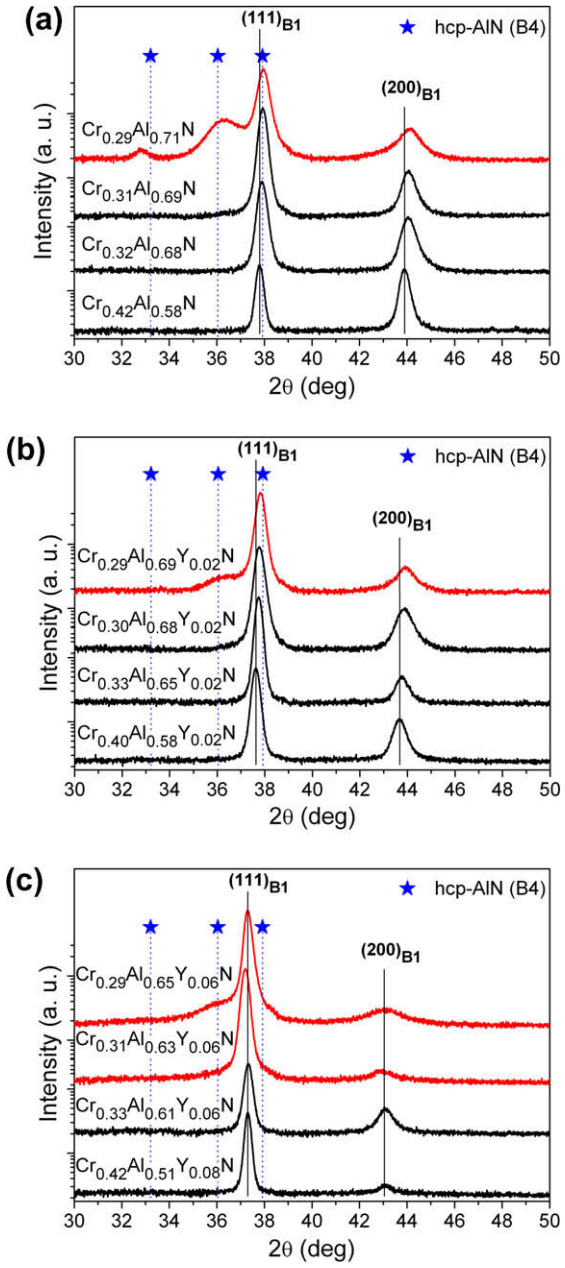

Fig. 4. X-ray diffraction patterns of magnetron sputtered $Cr_{1-x-y}Al_xY_yN$ films with varying Al- and Y contents.

parameter of 0.09 Å for CrAlN if the Al content is increased from $x = 0$ to 1 agrees well with the lattice parameter change of 0.07 and 0.11 Å reported in Refs. [18,40], where projector-augmented wave potentials within the Vienna ab initio simulation package [70–72] or exact muffin-tin orbitals within a Green's function technique [73–75] were used. Calculated bulk modulus data (Fig. 6b), on the other hand, exhibiting values from 230 to 270 GPa independent on the Al concentration, are in reasonable agreement with data presented elsewhere [16]. The decreasing bulk modulus with Y incorporation is in turn consistent with experimentally observed decreasing Young's moduli [65].

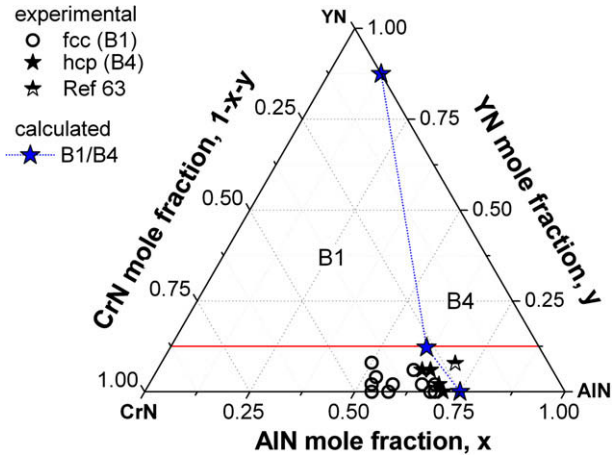

Fig. 5. Ab initio calculated (blue stars) and experimentally obtained (black circles designate the B1 structure, black stars the B4 structure) critical compositions where the B1–B4 transition occurs in $Cr_{1-x-y}Al_xY_yN$ within the ternary system CrN–AlN–YN. (For interpretation of the references to colour in this figure legend, the reader is referred to the web version of this article.)

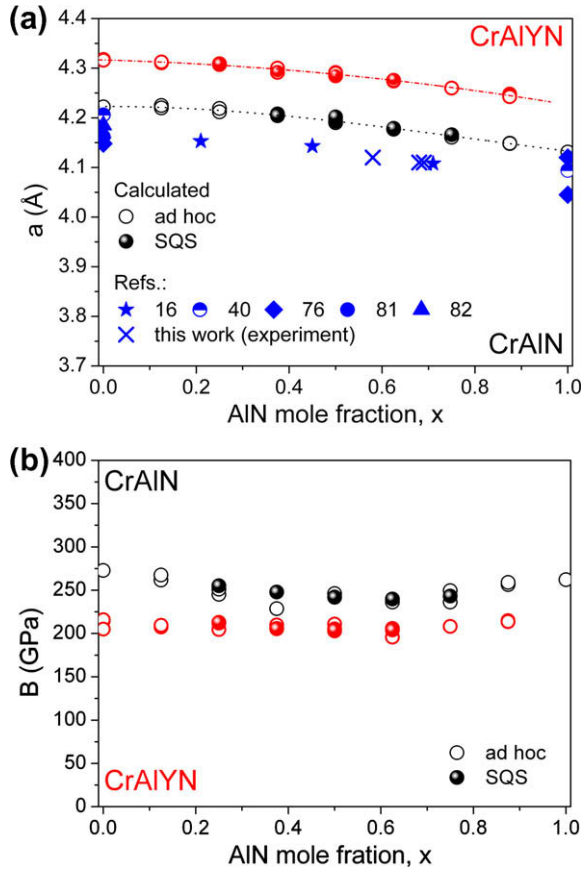

Fig. 6. Ab initio calculated (a) lattice parameters and (b) bulk moduli as a function of the AlN mole fraction x for fcc (B1) $Cr_{1-x}Al_xN$ and fcc (B1) $Cr_{0.875-x}Al_xY_{0.125}N$ as obtained from ad hoc and *SQS* supercells. Values reported and experimentally obtained in the literature are added for comparison.

4. Summary and conclusions

First-principles calculations of CrAlYN indicate that Y incorporation shifts the critical Al content, where B1/B4 transition occurs, from $x \approx 0.75$ for Y-free $Cr_{1-x}Al_xN$ to $x \approx 0.625$ for 6.25 at.% Y (12.5 mol.% YN; $y = 0.125$) containing $Cr_{0.875-x}Al_xY_{0.125}N$. This may be understood by considering the Y-induced changes in the electronic structure for the B1 and B4 structural modifications of the binary constituents CrN and AlN, respectively. The substitution of Cr by Y increases the cohesive energy (decreases the energy of formation) due to depletion of non-bonding (anti-bonding) states, which overcompensates lattice strain as a destabilizing contribution. Substitution of Al by Y, on the other hand, decreases the cohesive energy (increases the energy of formation) for Y additions up to approximate 60 mol.%, mainly due to lattice strain. Furthermore, Y incorporation into B1 AlN is energetically less favorable than Y incorporation into B4 AlN due to lattice strain. Hence, the stability of these cubic quaternary nitrides is reduced as Y is incorporated. The computational data are consistent with experimentally obtained critical Al contents of $x \approx 0.69$ for Y-free $Cr_{1-x}Al_xN$ and $x \approx 0.68$ and 0.61 for 1 and 3 at.% Y (2 and 6 mol.% YN; $y = 0.02$ and 0.06) containing $Cr_{1-x-y}Al_xY_yN$ films, respectively. Furthermore, the calculated mixing enthalpies of 0.26 and 0.24 eV atom^{-1} for fcc (B1) AlYN and fcc (B1) CrYN, respectively, suggest that Y equally substitutes for Cr or Al in a single-phase fcc (B1) CrAlYN structure. However, the somewhat lower mixing enthalpy of 0.18 eV atom^{-1} of hcp (B4) AlYN denotes that Y may temporarily be enriched in the hcp (B4) structure during decomposition of fcc (B1) CrAlYN into bcc (B2) Cr, hcp (B4) AlN, fcc (B1) YN and N_2.

Based on the results presented, critical Al contents of $x = 0.68$ are expected for 2 mol.% YN-containing cubic CrAlYN films, which exhibit the most promising oxidation resistance, as reported earlier. Consequently, it is envisioned that cubic CrAlYN films with maximized Al content ($Cr_{0.30}Al_{0.68}Y_{0.02}N$) yield a further improved oxidation performance. Larger Y- and/or Al contents promote the crystallization of the B4 structure and may cause nanocrystalline, partially X-ray-amorphous microstructures due to the simultaneous crystallization of the B1 and B4 phases.

Acknowledgements

This work was supported by the European Commission (project INNOVATIAL – Innovative processes and materials to synthesize knowledge-based ultra-performance nanostructured PVD thin-films on gamma titanium aluminides – NMP3-CT-2005-515884). J.M.S. acknowledges the financial support granted by Deutsche Forschungsgemeinschaft (DFG) within the project Schn. 735/14.

References

[1] Banakh O, Schmid PE, Sanjines R, Levy F. Surf Coat Technol 2003;163–164:57.
[2] Barshilia HC, Selvakumar N, Deepthi B, Rajam KS. Surf Coat Technol 2006;201:2193.
[3] Endrino JL, Fox-Rabinovich GS, Gey C. Surf Coat Technol 2006;200:6840.
[4] Kalss W, Reiter A, Derflinger V, Gey C, Endrino JL. Int J Refract Metals Hard Mater 2006;24:399.
[5] Knotek O, Loffler F, Scholl HJ. Surf Coat Technol 1991;45:53.
[6] Reiter AE, Brunner B, Ante M, Rechberger J. Surf Coat Technol 2006;200:5532.
[7] Reiter AE, Derflinger VH, Hanselmann B, Bachmann T, Sartory B. Surf Coat Technol 2005;200:2114.
[8] Spain E, Avelar-Batista JC, Letch M, Housden J, Lerga B. Surf Coat Technol 2005;200:1507.
[9] Chim YC, Ding XZ, Zeng XT, Zhang S. Thin Solid Films 2009;517:4845.
[10] Ding XZ, Tan ALK, Zeng XT, Wang C, Yue T, Sun CQ. Thin Solid Films 2008;516:5716.
[11] Hasegawa H, Kawate M, Suzuki T. Surf Coat Technol 2005;200:2409.
[12] Kaindl R, Franz R, Soldan J, Reiter A, Polcik P, Mitterer C, et al. Thin Solid Films 2006;515:2197.
[13] Kawate M. J Vac Sci Technol A 2002;20:569.
[14] Kimura A, Kawate M, Hasegawa H, Suzuki T. Surf Coat Technol 2003;169–170:367.
[15] Makino Y, Nogi K. Surf Coat Technol 1998;98:1008.
[16] Mayrhofer PH, Willmann H, Reiter AE. Surf Coat Technol 2008;202:4935.
[17] Sugishima A, Kajioka H, Makino Y. Surf Coat Technol 1997;97:590.
[18] Mayrhofer PH, Music D, Reeswinkel T, Fuß HG, Schneider JM. Acta Mater 2008;56:2469.
[19] Makino Y. Surf Coat Technol 2005;193:185.
[20] Zhang RF, Veprek S. Acta Mater 2007;55:4615.
[21] Rovere F, Mayrhofer PH, Reinholdt A, Mayer J, Schneider JM. Surf Coat Technol 2008;202:5870.
[22] Rovere F, Mayrhofer PH. J Vac Sci Technol A: Vac Surf Films 2008;26:29.
[23] Jedliński J. Oxid Metals 1993;39:55.
[24] Hovsepian PE, Reinhard C, Ehiasarian AP. Surf Coat Technol 2006;201:4105.
[25] Moser M, Mayrhofer PH, Clemens H. Intermetallics 2008;16:1206.
[26] Rovere F, Braun R, Schneider JM, Mayrhofer PH. Surf Coat Technol, submitted for publication.
[27] Moser M, Mayrhofer PH. Scripta Mater 2007;57:357.
[28] Hasegawa H, Suzuki T. Surf Coat Technol 2004;188–189:234.
[29] Hohenberg P, Kohn W. Phys Rev 1964;136:B864.
[30] Ozaki T. Phys Rev B 2003;67:155108.
[31] Blöchl PE. Phys Rev B 1990;41:5414.
[32] Troullier N, Martins JL. Phys Rev B 1991;43:1993.
[33] Perdew JP, Burke K, Ernzerhof M. Phys Rev Lett 1996;77:3865.
[34] Ozaki T, Kino H. Phys Rev B 2004;69:195113.
[35] Soler JM, Artacho E, Gale JD, Garcia A, Junquera J, Ordejon P, et al. J Phys: Condens Matter 2002:2745.
[36] Zunger A, Wei SH, Ferreira LG, Bernard JE. Phys Rev Lett 1990;65:353.
[37] Abrikosov IA, Niklasson AMN, Simak SI, Johansson B, Ruban AV, Skriver HL. Phys Rev Lett 1996;76:4203.
[38] Abrikosov IA, Simak SI, Johansson B, Ruban AV, Skriver HL. Phys Rev B 1997;56:9319.
[39] Cowley JM. J Appl Phys 1950;21:24.
[40] Alling B, Marten T, Abrikosov IA, Karimi A. J Appl Phys 2007;102:044314.

[41] Uv Barth, Hedin L. J Phys C: Solid State Phys 1972:1629.
[42] Kubler J, hock K-H, Sticht J, Williams AR. J Phys F: Metal Phys 1988;18:469.
[43] Oda T, Pasquarello A, Car R. Phys Rev Lett 1998;80:3622.
[44] Sandratskii LM. Adv Phys 1998;47:91.
[45] Theurich G, Hill NA. Phys Rev B 2001;64:073106.
[46] Birch F. J Geophys Res 1978;83:1257.
[47] Filippetti A, Hill NA. Phys Rev Lett 2000;85:5166.
[48] Nasr-Eddine M, Bertaut EF. Solid State Commun 1971;9:717.
[49] Corliss LM, Elliot N, Hastings JM. Phys Rev 1960;117.
[50] Ibberson RM, Cywinski R. Phys B: Phys Condens Matter 1992;180–181:329.
[51] Mavromaras A, Matar S, Siberchicot B, Demazeau G. J Magn Magn Mater 1994;134:34.
[52] Ney A, Rajaram R, Parkin SSP, Kammermeier T, Dhar S. Appl Phys Lett 2006;89.
[53] Music D, Sun Z, Ahuja R, Schneider JM. J Phys Condens Matter 2006;18:8877.
[54] Alling B, Karimi A, Abrikosov IA. Surf Coat Technol 2008;203:883.
[55] Rovere F, Music D, To Baben M, Fuss H-G, Mayrhofer PH, Schneider JM. J Phys D: Appl Phys, submitted for publication.
[56] Smirnova EA, Korzhavyi PA, Vekilov YK, Johansson B, Abrikosov IA. Eur Phys J B – Condens Matter Complex Syst 2002;30:57.
[57] Mayrhofer PH, Fischer FD, Böhm HJ, Mitterer C, Schneider JM. Acta Mater 2007;55:1441.
[58] Predel B. Li–Mg–Nd–Zr, Landolt–Börnstein – Group IV physical chemistry. Berlin: Springer-Verlag; 1997.
[59] Fernández Guillermet A, Häglund J, Grimvall G. Phys Rev B 1992;45:11557.
[60] Häglund J, Fernández Guillermet A, Grimvall G, Körling M. Phys Rev B 1993;48:11685.
[61] Xia Q, Xia H, Ruoff AL. J Appl Phys 1993;73:8198.
[62] De La Cruz W, Dáz JA, Mancera L, Takeuchi N, Soto G. J Phys Chem Solids 2003;64:2273.
[63] Scheerer H, Hoche H, Allebrandt D, Schramm B, Abele E, Berger C. Verschleißmechanismen von CrAlYN PVD Schichten bei Erhöhten Temperaturen 2007;38:356.
[64] Endrino JL, Derflinger V. Surf Coat Technol 2005;200:988.
[65] Rovere F, Mayrhofer PH. J Vac Sci Technol A: Vac Surf Films 2007;25:1336.
[66] Music D, Kölpin H, Baben M, Schneider JM. J Eur Ceram Soc 2009.
[67] Kittel C. Introduction to solid state physics. New York: Wiley; 2005.
[68] Mayrhofer PH, Music D, Schneider JM. J Appl Phys 2006;100:094906.
[69] Alling B, Karimi A, Hultman L, Abrikosov IA. Appl Phys Lett 2008;92:071903.
[70] Kresse G, Hafner J. Phys Rev B 1993;48:13115.
[71] Kresse G, Hafner J. Phys Rev B 1994;49:14251.
[72] Kresse G, Joubert D. Phys Rev B – Con Mat Mater Phys 1999;59:1758.
[73] Andersen OK, Saha-Dasgupta T. Phys Rev B – Condens Matter Mater Phys 2000;62:R16219.
[74] Vitos L. Phys Rev B – Condens Matter Mater Phys 2001;64:141071.
[75] Vitos L, Skriver HL, Johansson B, Kollár J. Comput Mater Sci 2000;18:24.
[76] Powder Diffraction File (Card 6-0694 for bfcc Cr, card 4-0787 for fcc Al, card 33-1458 for hcp Y, card 46-1200 and 25-1495 for fcc AlN, card 01-076-0702 for hcp AlN, card 01-077-047 for ffcc CrN, card 35-0779 for ffcc YN). International Center for Diffraction Data, JCPDF – ICDD 2005.
[77] Li C, Wu P. Chem Mater 2001;13:4642.
[78] Uehara S, Masamoto T, Onodera A, Ueno M, Shimomura O, Takemura K. J Phys Chem Solids 1997;58:2093.
[79] Zhang S, Chen N. Chem Phys 2005;309:309.
[80] Ueno M, Yoshida M, Onodera A, Shimomura O, Takemura K. Phys Rev B 1994;49:14.
[81] Gall D, Shin CS, Haasch RT, Petrov I, Greene JE. J Appl Phys 2002;91:5882.
[82] Hones P, Diserens M, Sanjines R, Levy F. J Vac Sci Technol B: Microelectron Nanometer Struct 2000;18:2851.
[83] Cherchab Y, Amrani B, Sekkal N, Ghezali M, Talbi K. Phys E: Low-Dimensional Syst Nanostruct 2008;40:606.